Transverse instabilities of deep-water solitary waves

Bernard Deconinck
Department of Applied Mathematics, University of Washington,
Campus Box 352420, Seattle, WA, 98195, USA

Dmitry E. Pelinovsky
Department of Mathematics, McMaster University
1280 Main Street West, Hamilton, Ontario, Canada, L8S 4K1

John D. Carter
Mathematics Department, Seattle University,
900 Broadway Seattle, WA 98122-4340

January 10, 2006

Abstract

The dynamics of a one-dimensional slowly modulated, nearly monochromatic localized wave train in deep water is described by a one-dimensional soliton solution of a two-dimensional nonlinear Schrödinger equation. In this paper, the instability of such a wave train with respect to transverse perturbations is examined numerically in the context of the nonlinear Schrödinger equation, using Hill's method. A variety of instabilities are obtained and discussed. Among these, we show that the solitary wave is susceptible to an oscillatory instability (complex growth rate) due to perturbations with arbitrarily short wavelength. Further, there is a cut-off on the instability with real growth rates. We show analytically that the nature of this cut-off is different from what is claimed in previous works.

1 Introduction

The hyperbolic nonlinear Schrödinger (NLS) equation in non-dimensional variables is

$$i\psi_t + \psi_{xx} - \psi_{yy} + 2|\psi|^2\psi = 0, \tag{1}$$

for a complex wave function $\psi(x, y, t)$. It describes the evolution of gravity-capillary waves in deep water that may be two-dimensional, nearly monochromatic, and are slowly modulated. Subscripts in (1) are used to denote partial derivatives. A derivation of this equation may be found in [2]. Up to scaling, the elevation of the water wave surface is given by

$$\eta = \Re\left(\psi e^{ik_0x - i\omega_0t}\right), \tag{2}$$

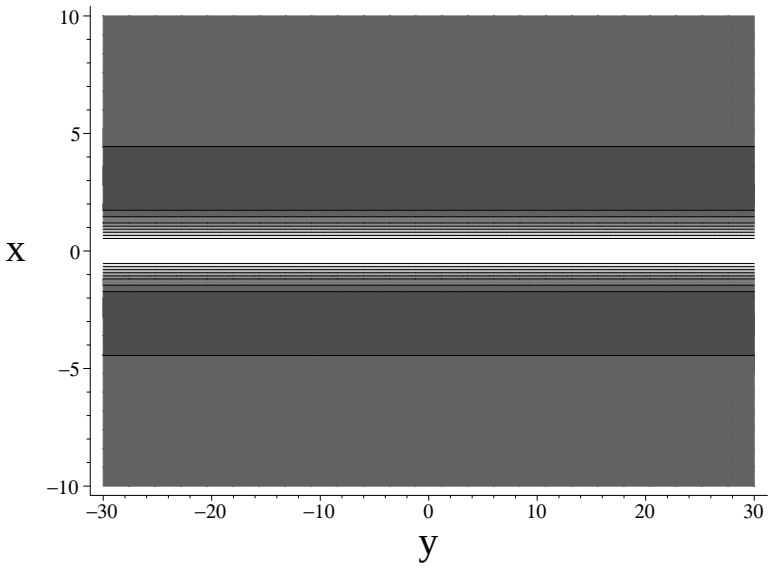

Figure 1: A contour plot of the water wave surface $\eta_0(x, y, t)$ with $k_0 = 1$, $t = 0$. Higher values correspond to lighter colors.

where $\Re$ denotes the real part, k_0 is the wave number of the carrier wave train, and $\omega_0 = \sqrt{k_0}$ is the carrier frequency given by the deep-water dispersion relation.

A trivial-phase one-soliton solution of the one-dimensional NLS equation (Eqn. (1), ignoring dependence on y) is given by

$$\psi = e^{it}\text{sech}x. \tag{3}$$

This solution corresponds to a one-dimensional localized wave train:

$$\eta_0(x, y, t) = \cos(k_0 x - (\omega_0 - 1)t)\text{sech}x. \tag{4}$$

A contourplot of $\eta_0(x, y, t)$ is shown in Fig. 1.

Remarks:

- By using the Lie point symmetries of (1) [23], this solution may be transformed into the most general form of a one-dimensional soliton solution with trivial spatial phase profile of (1). Thus, only considering (3) is not as restrictive as it appears.
- Using a linear transformation on the spatial variables, the solution (3) may be oriented so as to propagate at a non-zero angle with the x-axis [21]. The analysis of these solutions is similar to that considered here.

In order to examine the stability of (3) with respect to two-dimensional perturbations, consider

$$\psi = (\text{sech}x + \epsilon u(x, y, t) + i\epsilon v(x, y, t))\ e^{it} \tag{5}$$

where ϵ is a small, real constant and $u(x,y,t)$, $v(x,y,t)$ are real-valued functions. The resulting equation is polynomial in ϵ. Its constant term vanishes, since (3) is a solution of (1). The order ϵ term is dominant, and its coefficient is a linear partial differential equation for $u(x,y,t)$ and $v(x,y,t)$. Separating its real and imaginary parts gives the following coupled set of partial differential equations:

$$\left\{ \begin{array}{rcl} -u_t &=& v_{xx} - v_{yy} + \left(2\mathrm{sech}^2 x - 1\right) v \\ v_t &=& u_{xx} - u_{yy} + \left(6\mathrm{sech}^2 x - 1\right) u \end{array} \right. . \tag{6}$$

Since the coefficients of these equations do not explicitly depend on y or t, we may separate variables, and let

$$\left\{ \begin{array}{rcl} u(x,y,t) &=& U(x,\rho,\Omega) e^{i\rho y + \Omega t} + c.c. \\ v(x,y,t) &=& V(x,\rho,\Omega) e^{i\rho y + \Omega t} + c.c. \end{array} \right. , \tag{7}$$

where $\rho \in \mathbb{R}$, as only perturbations that are bounded in space are considered. Further, $+c.c.$ denotes that the complex conjugate of the previous term is added. Lastly, Ω is a complex constant that determines the stability of the solitary wave solution with respect to perturbations with x-dependence given by $U(x,\rho,\Omega)$ and $V(x,\rho,\Omega)$ and y-dependence characterized by the wave number ρ. Then $U(x,\rho,\Omega)$, $V(x,\rho,\Omega)$ satisfy the coupled system of ordinary differential equations

$$\left\{ \begin{array}{rcl} \Omega U &=& (L_- - \rho^2) V \\ -\Omega V &=& (L_+ - \rho^2) U \end{array} \right. , \tag{8}$$

where

$$\left\{ \begin{array}{l} L_- = -\partial_x^2 + 1 - 2\,\mathrm{sech}^2 x, \\ L_+ = -\partial_x^2 + 1 - 6\,\mathrm{sech}^2 x. \end{array} \right. . \tag{9}$$

Thus, if eigenfunctions $U(x,\rho,\Omega)$, $V(x,\rho,\Omega)$ of the system are found for which Ω has a strictly positive real part, the solitary wave solution (3) is unstable with respect to perturbations with wave number ρ. The growth rate of the perturbation is $\Re(\Omega)$. For real Ω, (U,V) are real-valued, and the form of the perturbed solution is

$$\eta_\epsilon = \eta_0 + 2\epsilon \cos(\rho y) e^{\Omega t} \left(U \cos(k_0 x - (\omega_0 - 1)t) - V \sin(k_0 x - (\omega_0 - 1)t\right). \tag{10}$$

This shows that a real positive eigenvalue Ω gives rise to uniform exponential growth of the perturbation, *i.e.,* the entire profile of the perturbation is multiplied by the same factor $e^{\Omega t}$. On the other hand, for complex Ω,

$$\begin{array}{rcl} \eta_\epsilon &=& \eta_0 + \epsilon e^{\Omega_R t} \Big(\Re(U + iV) \cos(k_0 x - (\omega_0 - 1)t + \rho y + \Omega_I t) - \\ && \Im(U + iV) \sin(k_0 x - (\omega_0 - 1)t + \rho y + \Omega_I t) + \Re(U - iV) \cos(k_0 x - (\omega_0 - 1)t - \rho y - \Omega_I t) + \\ && \Im(U - iV) \sin(k_0 x - (\omega_0 - 1)t - \rho y - \Omega_I t) \Big). \end{array} \tag{11}$$

In this case, the effect of the instability is not a mere amplification of the perturbation profile, as there is an additional oscillatory effect. We refer to instabilities due to non-real eigenvalues Ω as oscillatory instabilities.

In this paper, the spectral problem (8) is investigated numerically and analytically. A review of previous works on this problem is given in Section 2. The numerical results are discussed in Section 3. Sections 4 and 5 describe analytical results on the spectrum of (8). Section 6 concludes the paper. The Appendix contains the outline of the numerical method.

2 Literature review

An overview of previous work was already presented in [17]. For the sake of contrasting our results with those in the literature, this overview is partially repeated here, although different points are emphasized. Different reviews may be found in [25, 15, 14]. Similar considerations for a different but related problem are discussed in [22].

The transverse instability of the one-dimensional NLS equation soliton (3) was first discussed by Zakharov and Rubenchik [26] in 1974. The one-dimensional (*i.e.,* $\rho = 0$) problem (8) has a quadruple zero eigenvalue, *i.e.,* $\Omega = 0$ for $\rho = 0$. Zakharov and Rubenchik used regular perturbation theory near $(\rho, \Omega) = (0, 0)$ to find asymptotic expressions for four branches $\Omega(\rho)$. Two of these branches result in imaginary (neutrally stable) values of Ω, whereas the other two give a real positive (unstable) and a real negative (stable) value of Ω. In effect, this settles the global stability question of the one-dimensional soliton solution: it is unstable because it is unstable with respect to two-dimensional perturbations with long-wavelength (small ρ) transverse perturbations. The method of Zakharov and Rubenchik leads to

$$\Omega_1^2 = \frac{4}{3}\rho^2 - \frac{4}{9}\left(\frac{\pi^2}{3} - 1\right)\rho^4 + \mathrm{O}(\rho^6), \tag{12}$$

for the two real branches Ω_1 (unstable) and $-\Omega_1$ (stable), and

$$\Omega_2^2 = -4\rho^2 - \frac{4}{3}\left(\frac{\pi^2}{3} + 1\right)\rho^4 + \mathrm{O}(\rho^6), \tag{13}$$

for the two imaginary branches Ω_2 and $-\Omega_2$, both neutrally stable [3, 20, 14, 24].

Successively, attention focused on the transverse stability of (3) with respect to short waves (large ρ). Plotting the positive root of (12) may lead one to believe that there is a cut-off ρ_c on the set of ρ values for which (3) is unstable with respect to transverse perturbations with wave number ρ. However, this argument is based on a perturbation expansion around $(\rho, \Omega) = (0, 0)$, and is not valid for large ρ. Different authors examined this behavior, see for instance [6, 3, 21].

Cohen *et al.* (1976) [6] appear to be the first to consider (8) from a numerical point of view, for a large range of ρ values. Their results agree well with the perturbation result (12) for small values of ρ. For larger values of ρ they found that the instability growth rate due to real Ω reaches a maximum, around $\rho \approx 0.85$, after which it decreases. Their numerical results for values of $\rho > 1$ were sufficiently problematic that they were not displayed in their paper. Some unstable growth was observed for $\rho = 1.5$, but not for $\rho = 2$. At $\rho = 1$, they found that Ω is at around 90% of its maximal value.

Saffman & Yuen (1978) [21], apparently unaware of this work, solved the eigenvalue problem (8) numerically as well. They concluded that the growth due to real eigenvalues reaches a maximum around $\rho = 0.8$, after which it decreases to zero, at $\rho \approx 1.09$. Some of these results were extended

to periodic solutions with increasingly longer periods by Martin *et al.* [16]. These authors also discussed instabilities due to complex eigenvalues corresponding to short-wave (large ρ) perturbations, but no concrete claims about the soliton limit were made.

Anderson *et al.* (1979) [3] revisit earlier numerical results by Pereira *et al.* [20]. No references to [6] or [21] are made. Anderson *et al.* solve (8) numerically, using a leap-frog finite-difference method. They report excellent agreement with (12), almost up to the maximal value of Ω, obtained at $\rho \approx 0.8$. As ρ is advanced beyond $\rho = 1$, a bifurcation of the growth rate to complex values is observed, at $\rho \approx 1.08$. Their results are corroborated by use of the Rayleigh-Ritz variational quotient, using a variety of test functions.

Also in 1979, Ablowitz & Segur [1] considered this same problem, using mostly perturbation theory. Specifically, considering real Ω^2, they found that in the short-wave limit ($\rho \to \infty$), $\Omega^2 = -\rho^4 + \mathrm{O}(\rho^2)$. This establishes neutral stability at the leading order. These authors referred to experiments done in one-dimensional (*i.e.,* narrow) wave tanks by Hammack [9] at the University of Florida in 1979, which showed good agreement with the dynamics of (3) in a one-dimensional NLS equation setting. As the presence of transverse short-wave instabilities would appear to contradict these experimental observations, Ablowitz & Segur concluded that "short waves are not unstable. Indeed if they were, it would be difficult to observe envelope solitons even in narrow wave tanks."

Remarks

- It should be pointed out that many of the works discussed above claim to numerically solve the problem (8). In all cases, these authors presumably reduced (8) to a periodic problem, possibly with large period. The effect of this truncation is not discussed. The numerical method used in the present paper does this as well, but the effects due to a finite period are carefully controlled and can be made arbitrarily small by tuning the input parameters (see Appendix).

- The majority of the works cited are interested in the dominant unstable mode at any ρ. Starting from random perturbations, it is this mode which might be observed in experiments, or in numerical solutions of (1).

3 Numerical results

In this paper, the spectral problem (8) is solved numerically, for a discrete set of ρ-values, ranging from $\rho = 0$ to $\rho = 1.5$. The numerical method is described in the Appendix. The results of these numerical runs are presented in Figs. 2 and 3. Also indicated there are solid curves, depicting known and new analytical results. Note that Fig. 2a could be extended to stable modes, by including negative Ω. The resulting figure is reflection symmetric with respect to the horizontal axis. For values of $\rho > 1$, a spurious cloud of eigenvalues surrounds the eigenvalue $\Omega = 0$. This is a numerical effect. The size of this cloud can be made arbitrarily small by using larger values of L and N (see Appendix). For the runs here, $\Re(\Omega) < 0.02$ for any of the numerical eigenvalues in the spurious cloud. These points were removed before producing the plots shown here.

Fig. 4 displays the different bifurcations as ρ changes from $\rho = 0$ to $\rho = 1.5$. Note the fourfold symmetry due to the Hamiltonian character of (1). Finally, a variety of computed eigenfunctions

and the water wave surface they give rise to, using (10) or (11) is shown in Figs. 5, 6 and 7, corresponding to real and complex values of Ω.

From these figures the following conclusions may be drawn:

1. **Small-ρ instability:** as predicted by Zakharov and Rubenchik [26] (and verified by all cited in the previous section), as ρ moves away from 0, the quadruple eigenvalue at the origin splits in four, resulting in two real eigenvalues $\pm\Omega_1$ and two imaginary eigenvalues $\pm\Omega_2$. This is illustrated in Fig. 4a. The numerical results show excellent agreement with the perturbation results (12) and (13). A representative eigenfunction for the unstable eigenvalue Ω_1 is shown in Fig. 5i. As noted by Zakharov and Rubenchik, this eigenfunction is odd, and it gives rise to a so-called "snaking" instability, whereby the solitary wave ridge oscillates forward and backward.

   Also at $\rho = 0$, a discrete eigenvalue $\pm\Omega_3$ emerges from the edge point of each component of the continuous spectrum located at $\pm i(1 + k^2)$, with $k \in \mathbb{R}$. Note that Saffman & Yuen [21] already reported the emergence from the continuous spectrum at $\rho = 0$ of the isolated eigenvalue Ω_3. Such a bifurcation is known as an edge bifurcation. It may be analyzed using a modified Evans function [12, 13, 19].

2. **An oscillatory instability:** at $\rho \approx 0.31$, the isolated imaginary eigenvalues $\pm\Omega_2$ collide with the imaginary eigenvalues $\pm\Omega_3$. This gives rise to two complex conjugate pairs of eigenvalues $\pm\Omega_4(\rho)$ and $\pm\Omega_4^*(\rho)$, past $\rho \approx 0.3$, due to a Hamiltonian Hopf bifurcation. This bifurcation may be explained from the collision of eigenvalues of opposite (negative and positive) Krein signatures, where the Krein signature is the sign of the Hamiltonian of (6) computed for the eigenvector corresponding to the colliding imaginary eigenvalues [11].

   The real part of Ω_4 and Ω_4^* on these curves reaches a maximum at $\rho \approx 0.55$, after which it monotonically decreases. The corresponding eigenfunction and the resulting water wave surface are shown in Fig. 7vii. These eigenfunctions appear to be even, resulting in "neck" instability, where the ridge of the soliton alternates between being high and narrow, and low and broad. For all ρ, the growth rate $\Re(\Omega_4) = \Re(\Omega_4^*)$ along this curve is less than that of some other curve of unstable eigenvalues $\Omega(\rho)$ (*i.e.,* for any ρ in the domain of Ω_4, at least one other eigenvalue Ω exists such that $\Re(\Omega) > \Re(\Omega_4)$, see below). Thus this curve of complex eigenvalues and its eigenfunctions lead to oscillatory instabilities, but these are always dominated by other instabilities. The birth of these complex eigenvalues is illustrated in Fig. 4b. To our knowledge, the existence of the branch of oscillatory instabilities (complex eigenvalues) for the solitary wave solution (3) is a new result. Similar oscillatory instabilities for periodic waves were reported in [16].

3. **Maximal growth rate:** at $\rho \approx 0.8$, Ω_1 reaches its maximum $\Omega_1 \approx 0.657$, resulting in the largest growth rate for perturbations of the solution (3) of (1). For $\rho > 0.8$, Ω_1 decreases monotonically. This agrees qualitatively with the results in [6, 21] and quantitatively with [3]. A numerical computation of the resulting eigenfunction is shown in Fig 5ii. The resulting instability is still of snaking type.

4. **Behavior at $\rho = 1$:** the behavior at $\rho = 1$ has been the subject of much discussion. The

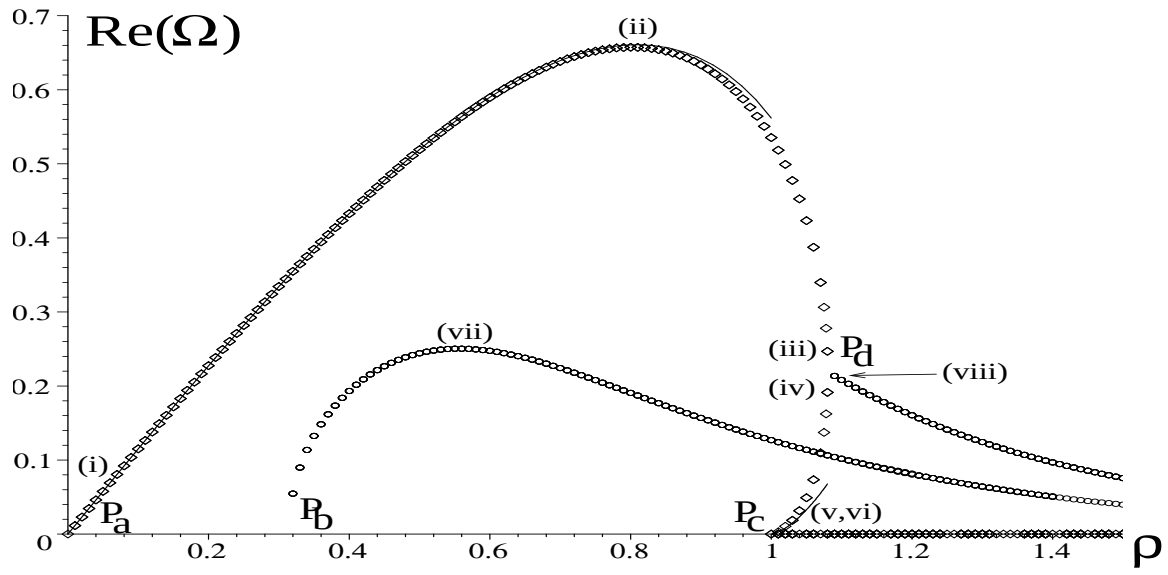

(a)

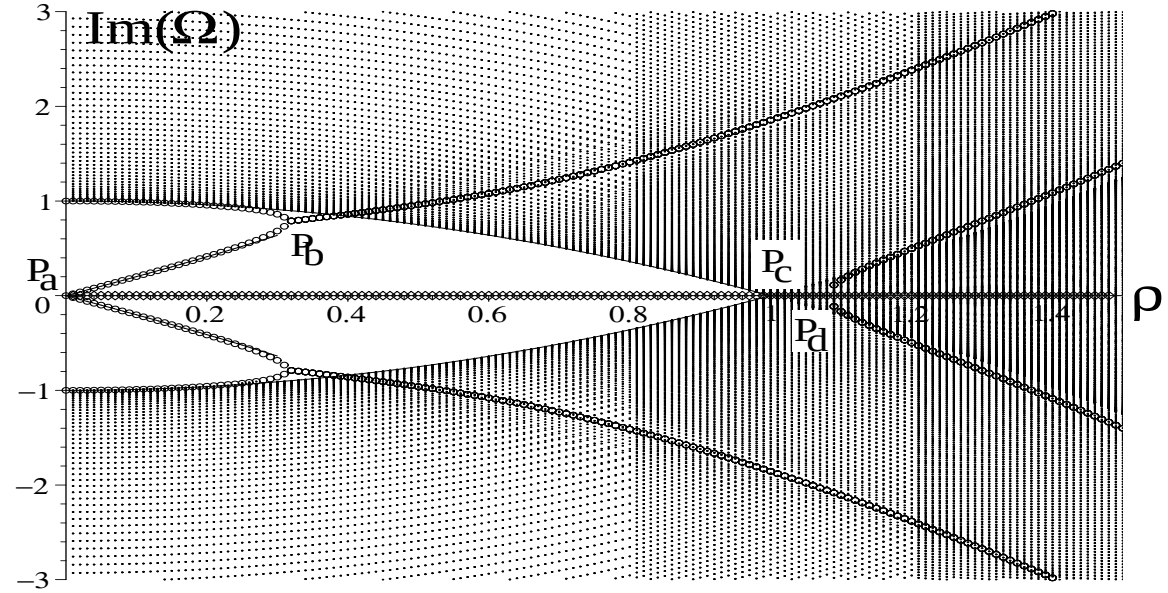

(b)

Figure 2: Real (a) and imaginary (b) parts of the spectrum of (8) as functions of varying ρ, obtained using the numerical method described in the Appendix. Also indicated are various analytical results, obtained using perturbation methods. Apart from the analytical results, all points plotted were computed numerically, and no filling in of one- or two-dimensional regions was done. The different bifurcation points of Fig. 4 are also indicated (P_a, P_b, P_c, P_d), as are the points corresponding to the eigenfunctions of Figs. 5-7. Points of the continuous spectrum are plotted as points, real discrete eigenvalues are shown as diamonds, complex discrete eigenvalues as circles. The solid line in Fig. (b) is the analytical result $\pm i(1-\rho^2)$, $\rho \leq 1$ for the boundary of the continuous spectrum.

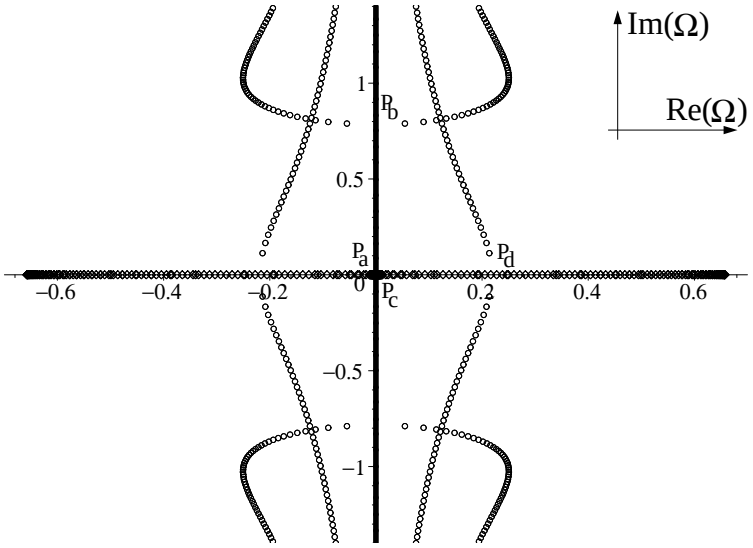

Figure 3: Ω spectrum of (8) for 150 equally-spaced values of $\rho \in [0, 1.5]$, obtained using the numerical method described in the Appendix. All points plotted were computed numerically, and no interpolation was done on the curves shown. The different bifurcation points of Fig. 4 are also indicated.

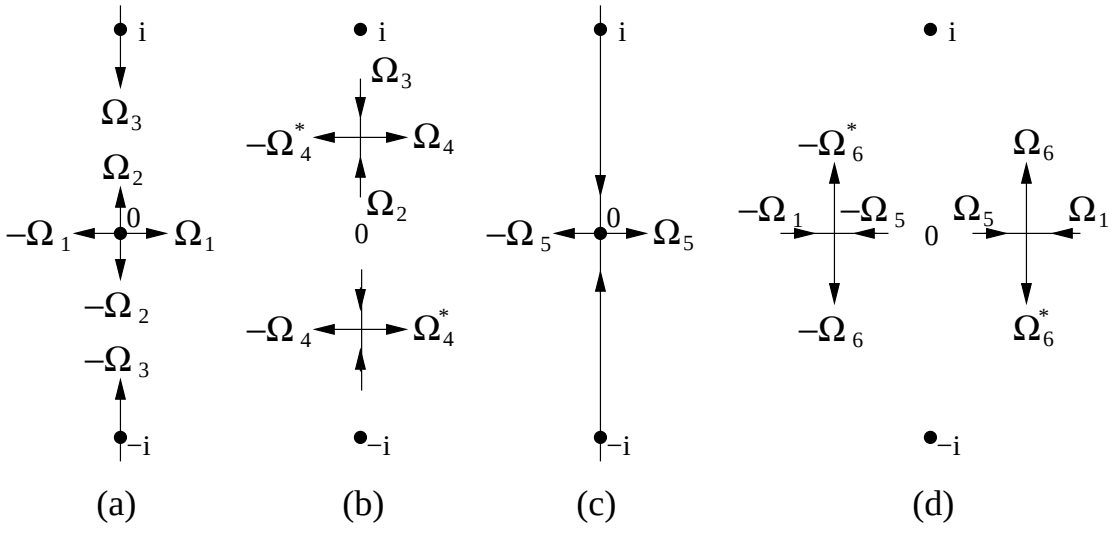

Figure 4: A conceptual picture of the bifurcations of discrete eigenvalues as a function of ρ in the complex Ω-plane. For (a) $\rho = 0$, (b) $\rho \approx 0.31$, (c) $\rho = 1$, and (d) $\rho \approx 1.08$. Arrows denote the change in Ω-values for increasing values of ρ.

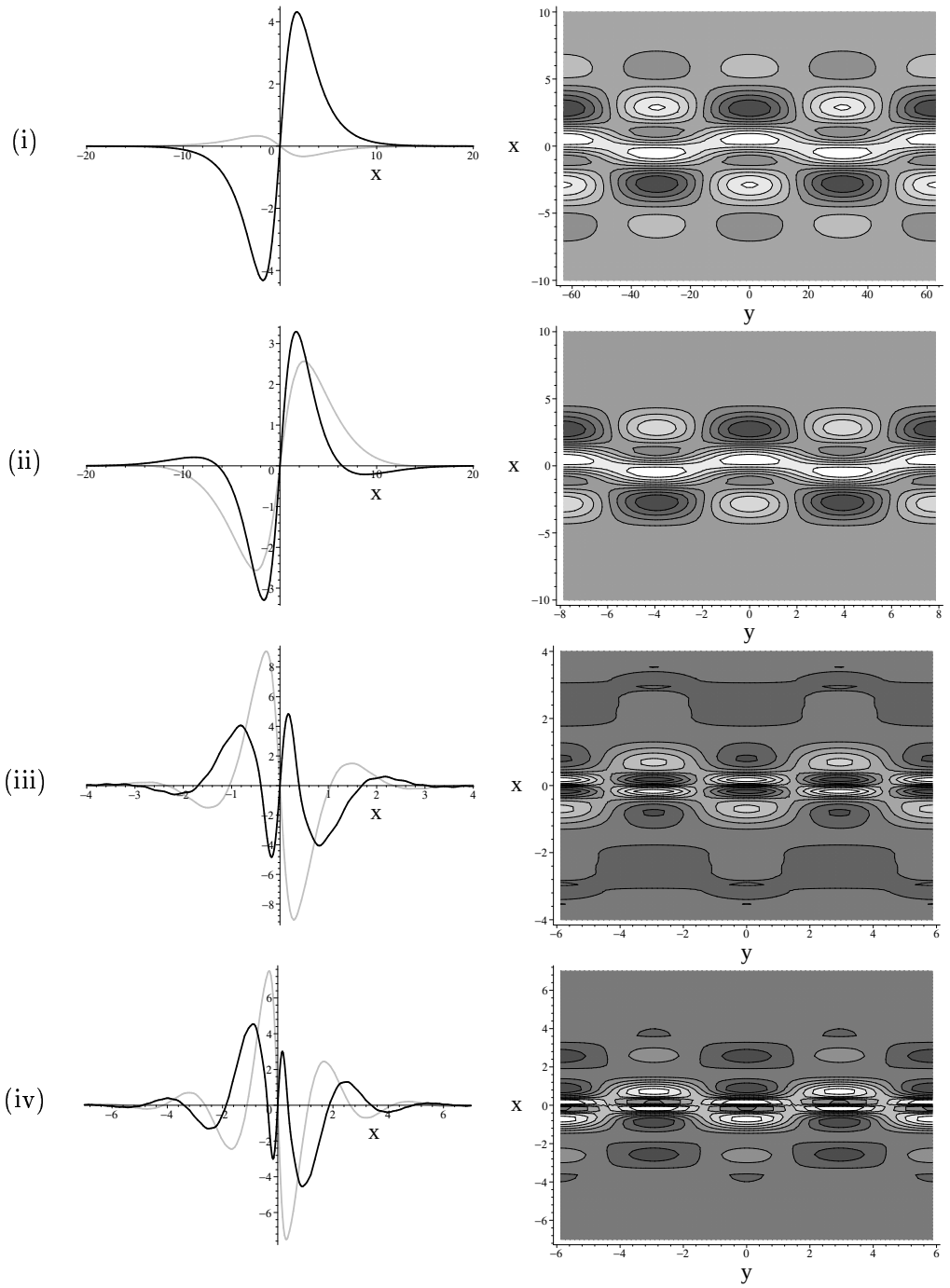

Figure 5: Numerically computed eigenfunctions (left) for real eigenvalues Ω. $U(x)$ is shown in black, $V(x)$ in grey. Also shown is a contour plot (right) of the water wave surface these eigenfunctions give rise to, using (10) and incorporating the contributions from (ρ, Ω) and $(\rho, -\Omega)$. Higher values correspond to lighter colors. Eigenfunctions are normalized so that $\sum_{k=-N}^{N} |U_k|^2 + |V_k|^2 = 1$. For all plots $\epsilon = 0.1$, $k_0 = 1$, $t = 0$ and $P = 2$. For (i) and (ii) the parameter values are $N = 100$ and $L = 50$. For (i) $(\rho, \Omega) = (0.1, 0.115)$, for (ii) $(\rho, \Omega) = (0.8, 0.657)$. For (iii) and (iv), $N = 500$, $L = 500$. For (iii) $(\rho, \Omega) = (1.07, 0.286454)$, for (iv) $(\rho, \Omega) = (1.07, 0.135085)$. The different scales on the axes in these figures should be noted.

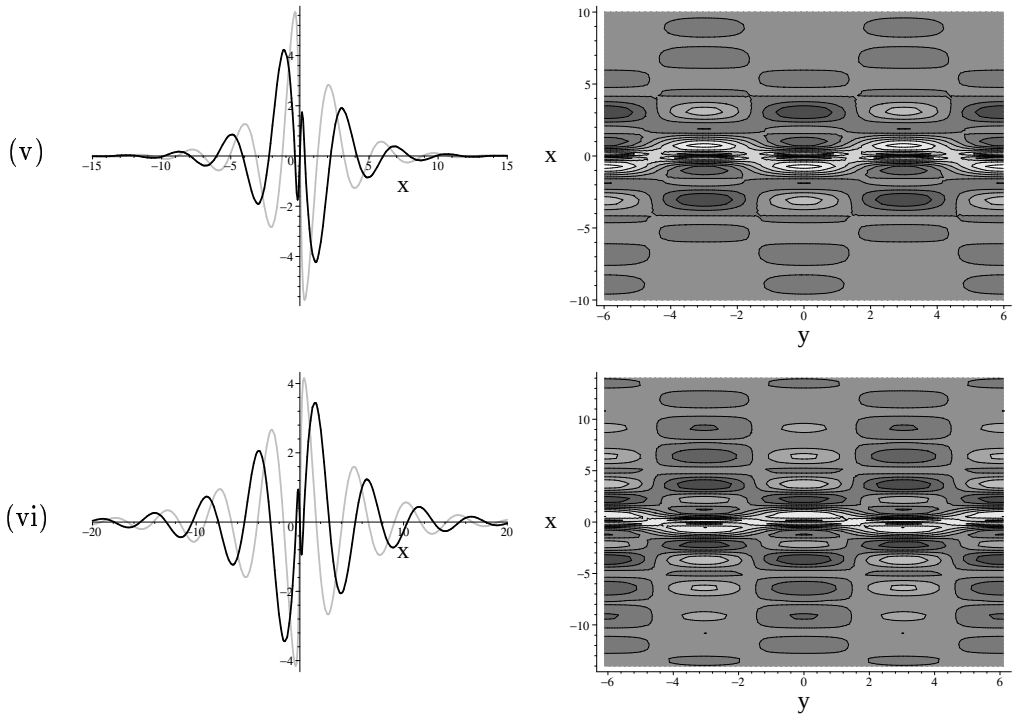

Figure 6: A continuation of the previous figure. For both (v) and (vi) $N = 500$, $L = 500$. For (v) $(\rho, \Omega) = (1.05, 0.0556098)$, for (vi) $(\rho, \Omega) = (1.03, 0.0205356)$.

continuous spectrum for (8) is always confined to the imaginary Ω axis. It may be found exactly by considering the behavior as $x \to \pm\infty$ in (8), leading to

$$\Omega_{\pm} = \pm i(1 - \rho^2 + k^2), \qquad k \in \mathbb{R} \tag{14}$$

as an explicit characterization of the continuous spectrum. Thus, for a given $\rho \geq 0$ the continuous spectrum is given by

$$\rho < 1 : \{\Omega \in \mathbb{C} : \Re(\Omega) = 0,\ \Im(\Omega) \geq 1 - \rho^2\} \cup \{\Omega \in \mathbb{C} :\ \Re(\Omega) = 0,\ \Im(\Omega) \leq -1 + \rho^2\} \tag{15a}$$

$$\rho \geq 1 : \{\Omega \in \mathbb{C} : \Re(\Omega) = 0\}. \tag{15b}$$

Note that the edge of the continuous spectrum is given by $\Omega_{\pm} = \pm i(1 - \rho^2)$. Our numerical results are in excellent agreement with this analytical result, as can be seen in Fig. 2b. At $\rho = 1$, the two previously disconnected parts of the continuous spectrum merge, after which they overlap for larger values of ρ. As depicted in Fig. 4c the consequence of this merger is the ejection of a pair of real eigenvalues $\pm\Omega_5$ for $\rho > 1$, given by

$$\Omega_5 = 2\sqrt{2}(\rho - 1)^{3/2} + \mathrm{O}((\rho - 1)^{5/2}), \tag{16}$$

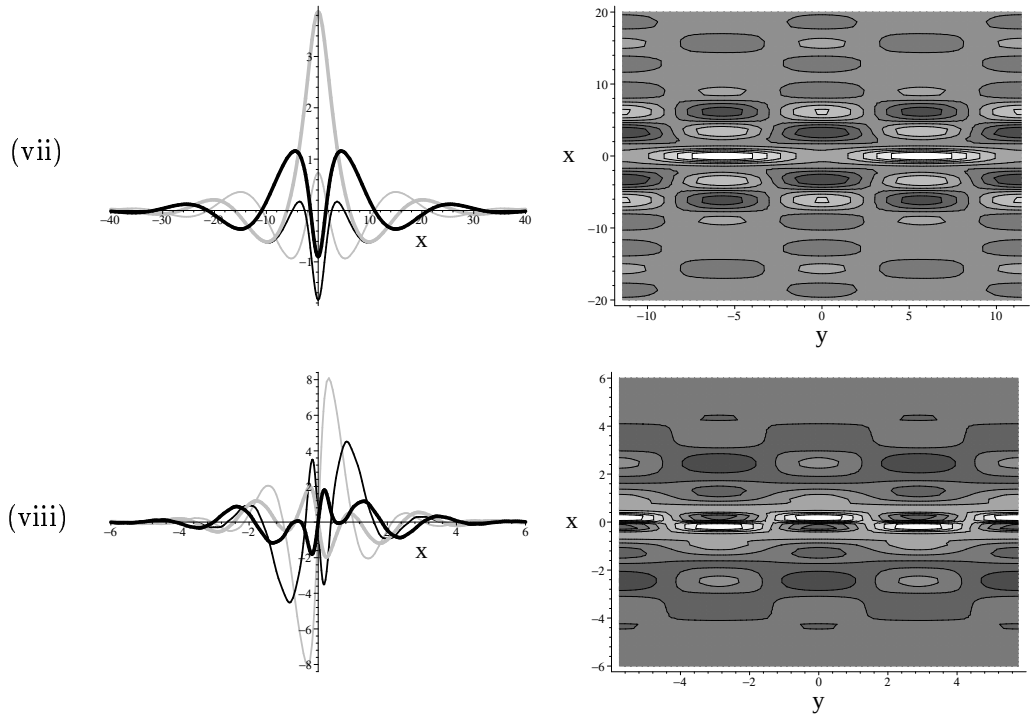

Figure 7: Numerically computed eigenfunctions (left) for complex eigenvalues Ω. $U(x)$ is shown in black, $V(x)$ in grey, real parts are shown with a thick line, imaginary parts with a thin line. Also shown is a contour plot (right) of the water wave surface these eigenfunctions give rise to, using (11) and incorporating the contributions from (ρ, Ω), $(\rho, -\Omega)$, (ρ, Ω^*) and $(\rho, -\Omega^*)$. Higher values correspond to lighter colors. All eigenfunctions are normalized so that $\sum_{k=-N}^{N} |U_k|^2 + |V_k|^2 = 1$. For all plots $\epsilon = 0.1$, $k_0 = 1$, $t = 0$ and $P = 2$. For (vii) the parameter values are $N = 100$ and $L = 50$, $(\rho, \Omega) = (0.55, 0.25 + 1.02\,i)$. For (viii), $N = 500$, $L = 500$, $(\rho, \Omega) = (1.09, 0.199897 + 0.143238\,i)$.

which is proven in Section 5. To our knowledge this is a new result. Two eigenfunctions on this branch are shown in Figs. 6v,vi.

5. **Existence of a cut-off for real Ω instabilities:** there is a largest ρ value ρ_c such that for $\rho > \rho_c$ no instabilities due to real $\Omega(\rho)$ exist. Approximately, $\rho_c \approx 1.08$. At ρ_c, the two eigenvalues Ω_1 and Ω_5 collide. Their corresponding eigenfunctions near the collision appear qualitatively similar. They are shown in Figs. 5iii,iv.

6. **Large-ρ instability:** the solitary wave is unstable with respect to perturbations with arbitrarily large transverse wave number ρ. This instability is due to a pair of complex conjugate eigenvalues (Ω_6, Ω_6^*) (emerging from the collision of Ω_1 and Ω_5 at ρ_c), as well as the pair of complex conjugate eigenvalues (Ω_4, Ω_4^*). For both branches $\Re(\Omega_6) > \Re(\Omega_4) > 0$, but $\Im(\Omega_6) \neq 0$, and thus the instability is oscillatory in nature. The behavior near $\rho = \rho_c$ is illustrated in Fig. 4d. This appears to be in agreement with the results of Anderson

et al. [3], and the results hinted at by Cohen *et al.* [6]. The eigenfunction corresponding to $(\rho, \Omega) = (1.09, 0.199897 + 0.143238\,i)$ and the resulting water wave surface are shown in Fig. 7viii. These eigenfunctions are odd, resulting in "snake" instability.

Note that the existence of a large-ρ instability does not contradict the conclusions reached by Ablowitz & Segur [1] because those authors only considered real Ω^2. It follows from their results that no *real* discrete eigenvalues exist for large ρ.

4 Bifurcations in the spectrum for $\rho^2 < 1$.

The spectra of the operators $L_\pm$ are known analytically. The continuous spectrum of $L_-\varphi = \lambda\varphi$ is $\{\lambda \in \mathbb{C} : \Re(\lambda) \geq 1\}$ and the discrete spectrum has an isolated eigenvalue at $\lambda = 0$. Similarly, the continuous spectrum of $L_+\varphi = \lambda\varphi$ is $\{\lambda \in \mathbb{C} : \Re(\lambda) \geq 1\}$ as well. In this case the discrete spectrum has two isolated eigenvalues at $\lambda = 0$ and at $\lambda = -3$.

When $0 < \rho^2 < 1$, the stability problem (8) satisfies the assumptions of the recent work [18]. Two negative eigenvalues of $L_+ - \rho^2$ and one negative eigenvalue of $L_- - \rho^2$ must match the unstable eigenvalues and the eigenvalues of negative Krein signature of the problem (8) (see Proposition 8.3 in [18]). Indeed, there is one real (unstable) eigenvalue Ω_1 and a pair of eigenvalues of negative Krein signatures $(\Omega_2, -\Omega_2)$ for $0 < \rho^2 < \rho_{c1}^2$, where $\rho_{c1} \approx 0.3$. (The fact that the pair $(\Omega_2, -\Omega_2)$ has negative Krein signature follows from Lyapunov–Schmidt reduction, see [22] for a similar analysis). The other pair of eigenvalues $(\Omega_3, -\Omega_3)$ has positive Krein signature, which follows from general properties of edge bifurcations [11]. The number of unstable eigenvalues (three total: one real and two complex) is preserved after the Hamiltonian–Hopf bifurcation for $\rho_{c1}^2 < \rho^2 < 1$.

5 Analysis of the behavior of the spectrum near $\rho^2 = 1$

It was previously hypothesized in the literature that the curve of the real unstable eigenvalue $\Omega_1(\rho)$ touches the horizontal axis at some cut-off value (see the discussion in [17]), and various values were mentioned (for example $\rho = 1.09$ in [21]), with $\rho = 1$ always being a contender. Our numerical results show that the curve $\Omega_1(\rho)$ does not touch the horizontal axis. Instead a new curve of eigenvalues $\pm\Omega_5$ emanates from the origin for $\rho > 1$ as a consequence of the collision of the two parts of the continuous spectrum, as mentioned in Section 3. Therefore, in this section, we prove the asymptotic formula (16).

When $\rho^2 > 1$, the assumptions of [18] are violated since the negative index of the operators $L_- - \rho^2$ and $L_+ - \rho^2$ becomes infinite. It was suggested in [17] that at $\rho^2 = 1$ a modified edge bifurcation takes place, which would be responsible for the disappearing of the unstable eigenvalues as ρ^2 is increased past 1. An analytical method was developed, based on eigenfunction decompositions and asymptotic analysis of singular integral equations (adopted from [19]). Unfortunately, a miscalculation was made. The integral kernel $K(k, k')$ defined below Eqn. (12) in [17] is singular in the limit $k, k' \to 0$, while it was assumed in Eq. (13) that $\lim_{k\to 0} \lim_{k'\to 0} K(k, k') = 0$. With this correction in mind, the results of Section 4 of [17] on the modified edge bifurcations cannot be justified. Note that the results of Section 5 of [17] remain valid, as they are based on regular perturbation theory.

In this section, we develop an alternative analysis based on the modified Evans function (following [12]). We confirm that the point $\rho^2 = 1$ does indeed give rise to a modified edge bifurcation, which leads to a new pair of real eigenvalues $(\Omega_5, -\Omega_5)$ for $\rho^2 > 1$, but to no additional eigenvalues for $\rho^2 < 1$.

5.1 The Evans function

In order to define the Evans function for the stability problem (8), we define a map from the parameters (ρ^2, Ω) to the new parameters (κ_+, κ_-),

$$\rho^2 = 1 - \frac{\kappa_+^2 + \kappa_-^2}{2}, \qquad \Omega = \frac{\kappa_+^2 - \kappa_-^2}{2\mathrm{i}}. \tag{17}$$

Near the point of interest $(\rho^2, \Omega) = (1, 0)$, the new parameters (κ_+, κ_-) provide a multiple cover of the original parameter plane (ρ^2, Ω). Using the new parameters, the Evans function can be locally extended in an analytic way. To find the eigenvalues of the stability problem (8), some care is required to ensure that the zeros of the extended Evans function are found on the correct Riemann sheet. Using the new parameters (κ_+, κ_-), the stability problem (8) is rewritten as

$$\left(-\partial_x^2 - 6\mathrm{sech}^2 x\right) U = -\frac{1}{2}(\kappa_+^2 + \kappa_-^2)U + \frac{i}{2}(\kappa_+^2 - \kappa_-^2)V, \tag{18a}$$

$$\left(-\partial_x^2 - 2\mathrm{sech}^2 x\right) V = -\frac{i}{2}(\kappa_+^2 - \kappa_-^2)U - \frac{1}{2}(\kappa_+^2 + \kappa_-^2)V. \tag{18b}$$

Let $\mathbf{u} = (U, U', V, V')^T$. The eigenfunctions corresponding to the discrete spectrum of (18a-b) decay exponentially as $e^{\kappa_\pm x}$ as $|x| \to \infty$ in the no-potential case. In the domain $\Re(\kappa_\pm) > 0$, we define four fundamental solutions of (18a-b) specified by their exponential behavior as $|x| \to \infty$:

$$\boldsymbol{u}_\pm(x; \kappa_+, \kappa_-) \to \begin{pmatrix} 1 \\ \kappa_\pm \\ \pm i \\ \pm i\kappa_\pm \end{pmatrix} e^{\kappa_\pm x}, \qquad \text{as} \quad x \to -\infty, \tag{19}$$

and

$$\boldsymbol{v}_\pm(x; \kappa_+, \kappa_-) \to \begin{pmatrix} 1 \\ -\kappa_\pm \\ \pm i \\ \mp i\kappa_\pm \end{pmatrix} e^{-\kappa_\pm x}, \qquad \text{as} \quad x \to +\infty. \tag{20}$$

The Evans function is defined as the Wronskian determinant of these fundamental solutions:

$$E(\kappa_+, \kappa_-) = \det\left(\boldsymbol{u}_+(x; \kappa_+, \kappa_-), \boldsymbol{u}_-(x; \kappa_+, \kappa_-), \boldsymbol{v}_+(x; \kappa_+, \kappa_-), \boldsymbol{v}_-(x; \kappa_+, \kappa_-)\right). \tag{21}$$

By Abel's theorem, this Wronskian determinant is independent of x. In the no-potential case, an easy calculation gives $E(\kappa_+, \kappa_-) = 16\kappa_+\kappa_-$. Following standard techniques (*e.g.* see [12]), the fundamental solutions (19-20) and the Evans function (21) are well-defined when the potential functions decay exponentially. Zeros (including multiplicities) of $E(\kappa_+, \kappa_-)$ in the domain $\Re(\kappa_+) > 0$ and $\Re(\kappa_-) > 0$ coincide with eigenvalues of the system (18a-b) with an exponentially decaying eigenfunction. The analyticity properties of $E(\kappa_+, \kappa_-)$ are described in the following proposition:

Proposition 1 *The fundamental solutions $\boldsymbol{u}_\pm(x;\kappa_+,\kappa_-)$ and $\boldsymbol{v}_\pm(x;\kappa_+,\kappa_-)$ characterized by (19-20) and the Evans function $E(\kappa_+,\kappa_-)$ defined by (21) are analytic functions near $(\kappa_+,\kappa_-)=(0,0)$.*

Proof. In the domain $\Re(\kappa_\pm)>0$, we express the fundamental solutions $\boldsymbol{u}_\pm(x;\kappa_+,\kappa_-)$ in the form:

$$\boldsymbol{u}_\pm(x;\kappa_+,\kappa_-)=\begin{pmatrix} u_\pm \\ u_\pm'+\kappa_\pm u_\pm \\ \pm i w_\pm \\ \pm i(w_\pm'+\kappa_\pm w_\pm)\end{pmatrix} e^{\kappa_\pm x}, \tag{22}$$

where the component functions $(u_\pm,w_\pm)$ solve the coupled system

$$\left(-\partial_x^2-6\mathrm{sech}^2 x\right)u_\pm = 2\kappa_\pm u_\pm' \pm i\Omega(u_\pm-w_\pm), \tag{23a}$$
$$\left(-\partial_x^2-2\mathrm{sech}^2 x\right)w_\pm = 2\kappa_\pm w_\pm' \mp i\Omega(u_\pm-w_\pm), \tag{23b}$$

subject to the boundary conditions

$$\lim_{x\to-\infty}u_\pm(x)=1,\quad \lim_{x\to-\infty}u_\pm'(x)=0,\quad \lim_{x\to-\infty}w_\pm(x)=1,\quad \lim_{x\to-\infty}w_\pm'(x)=0. \tag{24}$$

Since the system (23a-b) depends analytically on the parameters $(\kappa_+,\kappa_-)\in\mathbb{C}^2$ and the boundary conditions (24) are independent of (κ_+,κ_-), the fundamental solutions $\boldsymbol{u}_\pm(x;\kappa_+,\kappa_-)$ depend analytically on these parameters near the point $(\kappa_+,\kappa_-)=(0,0)$, see [8]. The same statement extends to the fundamental solutions $\boldsymbol{v}_\pm(x;\kappa_+,\kappa_-)$ and hence to the Evans function $E(\kappa_+,\kappa_-)$ computed at any $x\in\mathbb{R}$. ∎

5.2 Eigenvalues at $\Omega=0$

The point $\Omega=0$ corresponds to the case $\kappa_+^2=\kappa_-^2\equiv\kappa^2$, so that $\rho^2=1-\kappa^2$. We compute E_0, the value of $E(\kappa_+,\kappa_-)$ at $\kappa_+^2=\kappa_-^2$, to determine the possible values of ρ^2 at which bifurcations may occur. The value E_0 depends on whether $\rho^2>1$ or $\rho^2<1$.

For $\rho^2<1$ and $\Omega=0$, the system (8) decouples, and its solutions may be written in terms of the exact eigenfunctions of the operators L_- and L_+:

$$\boldsymbol{u}_\pm(x)=\begin{pmatrix} f_+ \\ f_+' \\ \pm i g_+ \\ \pm i g_+'\end{pmatrix},\quad \boldsymbol{v}_\pm(x)=\begin{pmatrix} f_- \\ f_-' \\ \pm i g_- \\ \pm i g_-'\end{pmatrix}, \tag{25}$$

where $(f_\pm,g_\pm)$ are given explicitly in [17] as

$$f_\pm(x) = \frac{2+q^2\mp 3q\tanh x-3\,\mathrm{sech}^2 x}{(1+q)(2+q)}e^{\pm qx},$$
$$g_\pm(x) = \frac{q\mp\tanh x}{1+q}e^{\pm qx},$$

with $q=\sqrt{1-\rho^2}>0$. It is easy to verify that (25) satisfies (19) and (20) with the correspondence $\kappa_+=\kappa_-=q$. Substituting (25) in the Evans function (21), we obtain the exact value of E_0 for $\rho^2<1$:

$$E_0 = 16q^2 \left(\frac{1-q}{1+q}\right)^2 \left(\frac{q-2}{q+2}\right), \qquad \text{with } q = \sqrt{1-\rho^2} > 0. \tag{26}$$

For $\rho^2 > 1$ and $\Omega = 0$, the fundamental solutions of (8) have another representation:

$$\boldsymbol{u}_\pm(x) = \begin{pmatrix} f_\pm \\ f'_\pm \\ \pm i g_\pm \\ \pm i g'_\pm \end{pmatrix}, \boldsymbol{v}_\pm(x) = \begin{pmatrix} \tilde{f}_\mp \\ \tilde{f}'_\mp \\ \pm i \tilde{g}_\mp \\ \pm i \tilde{g}'_\mp \end{pmatrix}, \tag{27}$$

where

$$\begin{aligned} f_\pm(x) &= \frac{k^2 - 2 \pm 3ik\tanh x + 3\,\mathrm{sech}^2 x}{(k \mp i)(k \mp 2\mathrm{i})} e^{\pm ikx}, \\ g_\pm(x) &= \frac{k \pm i\tanh x}{k \mp i} e^{\pm ikx} \end{aligned}$$

and

$$\begin{aligned} \tilde{f}_\pm(x) &= \frac{k^2 - 2 \pm 3ik\tanh x + 3\,\mathrm{sech}^2 x}{(k \pm i)(k \pm 2i)} e^{\pm ikx}, \\ \tilde{g}_\pm(x) &= \frac{k \pm i\tanh x}{k \pm i} e^{\pm \mathrm{i}kx}, \end{aligned}$$

with $k = \sqrt{\rho^2 - 1} > 0$. As before, it is easy to verify that (27) satisfies (19) and (20) with the correspondence $\kappa_+ = -\kappa_- = ik$. Substituting (27) in the Evans function (21), we obtain the exact value of E_0 for $\rho^2 > 1$:

$$E_0 = \frac{16k^4}{4 + k^2}, \qquad \text{with } k = \sqrt{\rho^2 - 1} > 0. \tag{28}$$

We see from (26) and (28) that $E_0 = 0$ at $\rho^2 = -3$, $\rho^2 = 0$, and $\rho^2 = 1$, which are the only bifurcation points from the origin $\Omega = 0$ (see also [17]). The first case ($\rho^2 = -3$) is not of interest here, because it results in an imaginary transverse wave number. Note that for the elliptic NLS equation this case corresponds to the cut-off on the range of transversely unstable wave numbers of the soliton solution (3), as shown by Janssen and Rasmussen [10]. The second case ($\rho^2 = 0$) has been analyzed in the past, originally by Zakharov & and Rubenchik [26], as reviewed in Section 2. We focus on the case $\rho^2 = 1$ in what follows.

5.3 Bifurcation analysis near $\rho^2 = 1$

The bifurcation point $\rho^2 = 1$ and $\Omega = 0$ corresponds to the origin $(\kappa_+, \kappa_-) = (0, 0)$ in the system (18a-b). Using Proposition 1, we study the Taylor series expansion of $E(\kappa_+, \kappa_-)$ near $(\kappa_+, \kappa_-) = (0, 0)$. Let the fundamental solutions $\mathbf{u}_\pm(x; \kappa_+, \kappa_-)$ be represented by (22). The Taylor series approximation for the scalar functions $(u_\pm, w_\pm)$ up to quadric terms in $\kappa_\pm$ can be written as

$$\begin{aligned} u_\pm = \quad & u_0(x) + \kappa_\pm u_1(x) + \kappa_\pm^2 u_2(x) + \kappa_\pm^3 u_3(x) + \kappa_\pm^4 u_4(x) \\ & \pm i\Omega \left(u_1^{(1)}(x) + \kappa_\pm u_2^{(1)}(x) + \kappa_\pm^2 u_3^{(1)}(x) \right) - \Omega^2 u_2^{(2)}(x) + \mathrm{O}(5), \end{aligned} \tag{29}$$

and

$$\begin{aligned} w_\pm = \quad & w_0(x) + \kappa_\pm w_1(x) + \kappa_\pm^2 w_2(x) + \kappa_\pm^3 w_3(x) + \kappa_\pm^4 w_4(x) \\ & \pm i\Omega \left(w_1^{(1)}(x) + \kappa_\pm w_2^{(1)}(x) + \kappa_\pm^2 w_3^{(1)}(x) \right) - \Omega^2 w_2^{(2)}(x) + \mathrm{O}(5), \end{aligned} \tag{30}$$

where Ω is defined by (17), and the terms O(5) represent the remainder of the Taylor series.

At zeroth order in $\kappa_\pm$, we find decoupled ordinary differential equations for the functions (u_0, w_0) satisfying the boundary conditions (24), so that

$$u_0 = 1 - \frac{3}{2}\,\mathrm{sech}^2 x, \qquad w_0 = -\tanh x. \tag{31}$$

The higher-order corrections solve a sequence of linear inhomogeneous problems with zero boundary conditions as $x \to -\infty$. The correction functions (u_n, w_n) solve the equations

$$\left(-\partial_x^2 - 6\mathrm{sech}^2 x\right) u_n = 2u_{n-1}', \tag{32a}$$

$$\left(-\partial_x^2 - 2\mathrm{sech}^2 x\right) w_n = 2w_{n-1}', \tag{32b}$$

for $n \geq 1$. The equations (32a-b) can be solved analytically, since all solutions with $\Omega = 0$ are known in closed form, see (25) and (27). For instance, the first few solutions of the inhomogeneous problems (32a) are found explicitly as follows:

$$u_1 = -\frac{3}{2}\left(1 + \tanh x - \frac{3}{2}\mathrm{sech}^2 x\right), \qquad w_1 = 1 + \tanh x \tag{33a}$$

$$u_2 = \frac{9}{4}\left(1 + \tanh x - \frac{3}{2}\mathrm{sech}^2 x\right) + \frac{3}{4}\mathrm{sech}^2 x, \qquad w_2 = -\left(1 + \tanh x\right) \tag{33b}$$

$$u_3 = -\frac{21}{8}\left(1 + \tanh x - \frac{3}{2}\mathrm{sech}^2 x\right) - \frac{9}{8}\mathrm{sech}^2 x, \qquad w_3 = 1 + \tanh x. \tag{33c}$$

The correction functions $(u_n^{(1)}, w_n^{(1)})$ solve the equations

$$\left(-\partial_x^2 - 6\mathrm{sech}^2 x\right) u_n^{(1)} = 2u_{n-1}^{(1)\prime} + u_{n-1} - w_{n-1}, \tag{34a}$$

$$\left(-\partial_x^2 - 2\mathrm{sech}^2 x\right) w_n^{(1)} = 2w_{n-1}^{(1)\prime} - u_{n-1} + w_{n-1}, \tag{34b}$$

for $n \geq 1$ and $u_0^{(1)} \equiv 0 \equiv w_0^{(1)}$. Since the homogeneous problems (34a-b) have non-zero solutions, solutions of the inhomogeneous problems with zero boundary conditions as $x \to -\infty$ grow algebraically as $x \to +\infty$. This follows easily from variation of parameters. For instance $(u_1^{(1)}, w_1^{(1)})$ grow as x^2, $(u_2^{(1)}, w_2^{(1)})$ grow as x^3, an so on. Similarly, the correction functions $(u_2^{(2)}, w_2^{(2)})$ satisfy inhomogeneous problems, from which it follows that these correction functions grow as x^4 in the limit $x \to +\infty$.

Replacing the other set of fundamental solutions $\boldsymbol{v}_\pm(x; \kappa_+, \kappa_-)$ by its asymptotic values (20) as $x \to +\infty$, we express the Evans function $E(\kappa_+, \kappa_-)$ in its explicit form (after some simplification):

$$E(\kappa_+, \kappa_-) = -\lim_{x \to +\infty} \begin{vmatrix} u_+ & u_- & 1 & 1 \\ u_+' + \kappa_+ u_+ & u_-' + \kappa_- u_- & -\kappa_+ & -\kappa_- \\ w_+ & -w_- & 1 & -1 \\ w_+' + \kappa_+ w_+ & -w_-' - \kappa_- w_- & -\kappa_+ & \kappa_- \end{vmatrix}. \tag{35}$$

The function $E(\kappa_+, \kappa_-)$ is expanded using the Taylor series expansions (29-30) for $(u_\pm, w_\pm)$ and the explicit analytical solutions (31), (33a–c). Explicit computations using symbolic manipulations in either Maple or Mathematica results in

$$\begin{aligned} E(\kappa_+, \kappa_-) = \; & -4(\kappa_+ + \kappa_-)^2 + 10(\kappa_+ + \kappa_-)^3 - 13(\kappa_+^4 + \kappa_-^4) - 51(\kappa_+^2 + \kappa_-^2)\kappa_+\kappa_- - 72\kappa_+^2\kappa_-^2 \\ & -\alpha_0(\kappa_+^2 - \kappa_-^2)^2 + \mathrm{O}(5), \end{aligned} \tag{36}$$

where α_0 is a numerical coefficient, given by

$$\alpha_0 = \lim_{x \to +\infty} \left(\frac{3}{2} u_1^{(1)\prime} + u_2^{(1)\prime} - \frac{7}{2} w_1^{(1)\prime} - w_2^{(1)\prime} + u_1^{(1)\prime} w_1^{(1)\prime} \right). \tag{37}$$

Although the correction functions $(u_1^{(1)}, w_1^{(1)})$ and $(u_2^{(1)}, w_2^{(1)})$ grow algebraically as $x \to +\infty$, one readily shows using the inhomogeneous problems (34a-b) that the algebraically growing terms cancel and a finite value for α_0 exists. This fact is also implied from Proposition 1, since the function $E(\kappa_+, \kappa_-)$ is well-defined, x-independent and analytic for small $\kappa_\pm$. Let us define new variables

$$\alpha = \kappa_+ + \kappa_-, \qquad \beta = \kappa_+ - \kappa_-. \tag{38}$$

This allows us to rewrite the Taylor series approximation (36) using these variables (α, β) as

$$E(\alpha, \beta) = -4\alpha^2 + 10\alpha^3 - \frac{25}{2}\alpha^4 + \frac{1}{4}\beta^4 - \left(\alpha_0 + \frac{3}{4} \right) \alpha^2 \beta^2 + \mathrm{O}(5). \tag{39}$$

The main consequence for our purposes of the Taylor series approximation is formulated below.

Proposition 2 *There exists only one family of zeros of $E(\alpha, \beta) = 0$ in a local neighborhood of the point $(\alpha, \beta) = (0, 0)$. This family of zeros is given asymptotically by*

$$\alpha^2 = \frac{1}{16}\beta^4 + \mathrm{O}(\beta^6) \tag{40}$$

Proof. Since $E(\alpha, \beta)$ is analytic near $(\alpha, \beta) = (0, 0)$, all zeros of $E(\alpha, \beta)$ in a neighborhood of $(0, 0)$ may be obtained using the Newton polygon technique (see Section 2.8 in [4]). Constructing the convex Newton polygon from the fourth-order terms (39), we obtain only one line segment, namely between the terms α^2 and β^4, which proves the leading-order result (40) by invoking the Implicit Function Theorem (see Section 2.2 in [4]), modulo the actual coefficient of β^4, which is easily found using a regular scaling argument.

In order to prove that the next-order term in (40) is on the order of $\mathrm{O}(\beta^6)$, we need to prove that the term β^5 is absent in the remainder $O(5)$ terms of the expansion (39). Since this term should also be present if we let $\alpha = 0$, this may be inferred from the exact solution (28) for $\Omega = 0$. Indeed, for that case we have $k = \sqrt{\rho^2 - 1}$, with $\kappa_+ = ik$, $\kappa_- = -ik$, $\alpha = 0$, and $\beta = 2ik$. Since the expression (28) is even in k, the term k^5 is absent, therefore the term with β^5 is absent from (39). ∎

5.4 Proof of the asymptotic formula (16)

The inverse mapping of (17) is

$$\kappa_\pm = \sqrt{1-\rho^2 \pm i\Omega}, \tag{41}$$

where we consider the right half-plane of the complex plane of Ω. The two branches of the square root function are defined as usual:

$$\sqrt[\pm]{z} = \pm\sqrt{|z|}e^{i\arg(z)/2}, \quad \forall z \in \mathbb{C}, \tag{42}$$

with $\arg(z) \in [0, 2\pi)$. When $\rho^2 < 1$, $\Re(\Omega) > 0$, and $|\Im(\Omega)| < (1-\rho^2)$, the numbers $1-\rho^2 \pm i\Omega$ lie in the first $(+)$ and fourth $(-)$ quadrants of the complex plane. When $\rho^2 > 1$, $\Re(\Omega) > 0$, and $|\Im(\Omega)| < \rho^2 - 1$, the numbers $1-\rho^2 \pm i\Omega$ lie in the second $(+)$ and third $(-)$ quadrants. For both of these cases, the $+$ square root function (42) is used for the mapping κ_+ and the $-$ square root function is used for the mapping κ_-. Thus, κ_+ maps to the first quadrant, while κ_- maps to the fourth quadrant. Since the new eigenvalue Ω_5 is real, we only need to consider the mappings $\kappa_\pm$ in a narrow strip $|\Im(\Omega)| < |1-\rho^2|$ around the real axis, as above. Thus, the parameters α and β in Proposition 2 are defined explicitly in terms of ρ and Ω as

$$\alpha = \sqrt[+]{1-\rho^2+i\Omega} + \sqrt[-]{1-\rho^2-i\Omega}, \tag{43a}$$

$$\beta = \sqrt[+]{1-\rho^2+i\Omega} - \sqrt[-]{1-\rho^2-i\Omega}. \tag{43b}$$

The balance in (40) implies that $|\Omega|$ can not be of order $|1-\rho^2|$ as $\rho^2 \to 1$. Therefore, we consider three separate cases, when $|\Omega|$ is of different orders in $|1-\rho^2|$ and the definitions of α and β can be simplified.

Case I: Let $k = \sqrt{\rho^2-1} \geq 0$ and $|\Omega| < k^2$. The Taylor series expansions of the mappings (43a-b) converge and result in

$$\alpha = \frac{\Omega}{k}\left(1 + \mathrm{O}\left(\frac{\Omega^2}{k^4}\right)\right), \qquad \beta = 2ik\left(1 + \mathrm{O}\left(\frac{\Omega^2}{k^4}\right)\right).$$

With this expansion, the asymptotic result (40) is equivalent to the pair of real eigenvalues

$$\Omega = \pm k^3 + \mathrm{O}(k^5).$$

Therefore, we have established an asymptotic approximation for the real unstable eigenvalue $\Omega_5(\rho)$, bifurcating for $\rho^2 > 1$ from the point $(\rho, \Omega) = (1, 0)$:

$$\Omega_5 = (\rho^2-1)^{3/2} + \mathrm{O}((\rho^2-1)^{5/2}) = 2\sqrt{2}\,(\rho-1)^{3/2} + \mathrm{O}((\rho-1)^{5/2}). \tag{44}$$

Case II: Let $q = \sqrt{1-\rho^2} \geq 0$ and $|\Omega| < q^2$. Then the Taylor series expansions of the mappings (43a-b) converge and give

$$\alpha = 2q\left(1 + \mathrm{O}\left(\frac{\Omega^2}{q^4}\right)\right), \qquad \beta = \frac{i\Omega}{q}\left(1 + \mathrm{O}\left(\frac{\Omega^2}{q^4}\right)\right).$$

Using this expansion, the asymptotic result (40) is equivalent to four eigenvalues defined by

$$\Omega^2 = \pm 8q^3 + \mathrm{O}(q^4).$$

However, the scaling $|\Omega| = \mathrm{O}(q^{3/2})$ violates the assumption that $|\lambda| < q^2$ as $q \to 0$. Therefore, this case does not produce non-zero eigenvalues of the discrete spectrum.

Case III: Let $|\Omega| > |1 - \rho^2|$. The Taylor series expansions of the mappings (43a-b) converge and result in

$$\begin{aligned} \alpha &= i\sqrt{2|\Omega|}e^{i\theta/2}\left(1 + \mathrm{O}\left(\frac{1-\rho^2}{\Omega}\right)\right), \\ \beta &= \sqrt{2|\Omega|}e^{i\theta/2}\left(1 + \mathrm{O}\left(\frac{1-\rho^2}{\Omega}\right)\right), \end{aligned}$$

where $\theta = \arg(\Omega)$. With this expansion the asymptotic result (40) produces only one solution $\Omega = 0$, which is consistent with the assumptions only if $q = 0$. Therefore, this case does not produce non-zero eigenvalues of the discrete spectrum either.

The above analysis proves the following theorem.

Theorem *The modified edge bifurcation for the stability problem (8) at $\rho^2 = 1$ results in a pair of discrete eigenvalues $(\Omega_5, -\Omega_5)$ in the domain $\rho^2 > 1$ given by the asymptotic approximation (16). No eigenvalues bifurcate from $\Omega = 0$ at $\rho^2 = 1$ into the domain $\rho^2 < 1$.*

The result (44) is plotted in Figs. 2 and 8 as a solid curve. Figure 8 shows the real parts of eigenvalues zoomed near the point $\rho = 1$. This figure illustrates the correctness of the asymptotic approximation (44), but it also demonstrates its small range of validity. This is somewhat expected. First, (44) is a low-order approximation. The inclusion of higher-order terms should improve the range of validity of the approximation. Second, at $\rho \approx 1.08$ the bifurcation $(\Omega_1, \Omega_5) \to (\Omega_6, \Omega_6^*)$ takes place, and one cannot expect the approximation (44) to be valid near or beyond where this other bifurcation occurs.

6 Concluding remarks

In this paper we have considered the linear stability problem (8), for the parameter $\rho \in [0, 1.5]$. We have considered both real and complex eigenvalues, and the discrete and the continuous spectrum were computed. Wherever both are available, the agreement between numerical and analytical results is excellent, serving to validate both.

From the point of physical applications, the most important result presented in this paper is the existence of Ω_4 and Ω_6, which implies the instability of the one-dimensional NLS soliton (3) with respect to perturbations of all wave lengths, including arbitrarily short ones. As outlined in Section 2, it was known previously that (3) is unstable with respect to long-wave (small-ρ) perturbations. Instabilities with respect to short-wave (large-ρ) perturbations were first hinted at by Cohen *et al.* [6]. The presence of such oscillatory instabilities was shown in more detail by Anderson *et al.* [3].

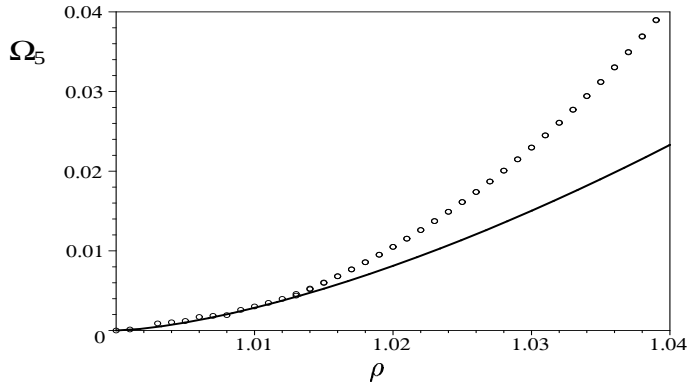

Figure 8: The unstable eigenvalue Ω_5 of the stability problem (8) as a function of the parameter ρ near $(\rho, \Omega) = (1, 0)$. The asymptotic result (44) is shown as a solid curve. The numerical results are shown as dots.

How is this consistent with the remarks of Ablowitz & Segur [1]? They state that the observations of Hammack [9] imply the stability of (3) with respect to short-wave perturbations. This issue may be resolved by a closer look at Fig. 2a. It is clear from that figure that the growth rate associated with such instabilities is smaller by an approximate factor of at least 4: the maximal growth rate at $\rho = 0.8$ is approximately 0.657. The largest growth rate associated with Ω_6 is approximately 0.2 at $\rho = \rho_c$. The experiments performed by Hammack [9] were done in a long, narrow wave tank. In such a setting, the smallest value of ρ resulting in a transverse perturbation of wave length $\lambda = 2\pi/\rho$ that will fit in the transverse direction of the wave tank is found significantly beyond the critical value $\rho_c \approx 1.08$. For those values of ρ, the associated growth rate is small, and observing this instability experimentally is difficult. One possibility is to employ a longer or wider tank, which is not a practical suggestion. The other possibility is to seed the instability by letting the wave pattern evolve according to (11), as opposed to according to (3). This might be accomplished using a suitably shaped paddle at the wave maker.

From a mathematical point of view, the main result of this paper is the bifurcation of the eigenvalues $(\Omega_5, -\Omega_5)$ from the continuous spectrum, at the parameter value $\rho = 1$ before which both parts of the continuous spectrum are disconnected. This result was established both numerically and analytically, resulting in the asymptotic approximation (44).

Mathematically, it would be desirable to also have asymptotic approximation results for the discrete but complex eigenvalue branches Ω_4 and Ω_6. Since these bifurcations do not occur from the origin, the analysis near their point of origin may be more complicated. Since for both Ω_4 and Ω_6 the imaginary part $\to \infty$ as $\rho \to \infty$, it seems reasonable that one may be able to establish a large ρ result, valid near the point at infinity on the complex Ω sphere.

Appendix: The numerical method

The numerical method used to solve (8) is in essence due to Hill, who used it for the study of the equation that now bears his name. The method is discussed in extensive detail in [7]. It is

especially suitable for equations with periodic coefficients. In this paper, we restrict the infinite-line problem to the interval $x \in [-L, L]$. This restriction is then periodically extended. For all numerical simulations, it is essential to ensure that a sufficiently large value of L has been used. This is easily verified by examining the degeneration of periodic bands to isolated eigenvalues.

For $x \in [-L, L]$,

$$\operatorname{sech}^2 x = \sum_{n=-\infty}^{\infty} S_n e^{in\pi x/L}, \tag{45}$$

with

$$S_n = \frac{1}{2L} \int_{-L}^{L} e^{-in\pi x/L} \operatorname{sech}^2 x \, dx. \tag{46}$$

Next, we assume that both U and V are periodic with period $2LP$, where P is a positive integer. Letting $P = 1$ gives rise to perturbations that have the same period as the truncated coefficient, $P = 2$ allows for period and anti-periodic perturbations, and so on. Further, an overall multiplicative phase factor may be present as well, according to Floquet theory [5, 7]. Thus

$$\begin{cases} U(x, \rho, \Omega) &= e^{i\mu x} \displaystyle\sum_{n=-\infty}^{\infty} U_n e^{in\pi x/LP}, \\ V(x, \rho, \Omega) &= e^{i\mu x} \displaystyle\sum_{n=-\infty}^{\infty} V_n e^{in\pi x/LP}, \end{cases} \tag{47}$$

with $\mu \in [-\pi/2LP, \pi/2LP)$, and

$$\begin{cases} U_n = \dfrac{1}{2LP} \displaystyle\int_{-LP}^{LP} e^{-in\pi x/LP} U(x, \rho, \Omega) e^{-i\mu x} \, dx, \\ \\ V_n = \dfrac{1}{2LP} \displaystyle\int_{-LP}^{LP} e^{-in\pi x/LP} V(x, \rho, \Omega) e^{-i\mu x} \, dx. \end{cases} \tag{48}$$

These series are substituted in (8). First, the common factor of $e^{i\mu x}$ is canceled, after which the coefficients of all distinct exponentials are equated to zero. This gives rise to the coupled bi-infinite difference equations

$$\begin{cases} \left(\left(\mu + \dfrac{n\pi}{LP} \right)^2 + 1 - \rho^2 \right) V_n - 2 \displaystyle\sum_{k=-\infty}^{\infty} S_{(n-k)/P} V_k &= \Omega \, U_n, \\ \left(\left(\mu + \dfrac{n\pi}{LP} \right)^2 + 1 - \rho^2 \right) U_n - 6 \displaystyle\sum_{k=-\infty}^{\infty} S_{(n-k)/P} U_k &= -\Omega \, V_n, \end{cases} \tag{49}$$

for $n \in \mathbb{Z}$. In these equations $S_{(n-k)/P} = 0$ unless $n - k$ is divisible by P. In order to use these bi-infinite difference equations as the basis for a numerical method, they are truncated to incorporate only $n = -N, \ldots, N$, for some positive integer N. Thus, for any simulation, two numerical choices need to be made: the period $2L$ at which $\operatorname{sech}^2 x$ is cut off, and the truncation on the number N of

Fourier modes used in (49). Two more algorithm choices are required as well: which value of P is used, and which values of μ are used. Once these parameters are fixed, the QR algorithm is used to find the eigenvalues Ω of the resulting $(4N+2)\times(4N+2)$-dimensional matrix. This is repeated for any choice of μ and ρ. These eigenvalues give approximations to elements of the spectrum of (8). Any desired corresponding eigenfunctions are easily recovered from the corresponding eigenvectors.

This numerical method certainly has its limitations. Many of these are discussed in [7], but one also finds there a discussion of many advantages of the method, such as its spectral convergence and its ability to approximate the entire spectrum in a compact region of the complex plane. In the context of this problem, the method should be compared with the other methods that have been employed, as discussed in Section 2. Many of those are continuation methods which work well in many respects, but they only give one branch of the spectrum if there are multiple ones. Further, if the spectral branches have vertical tangents as functions of ρ, continuation methods used carelessly may either break down or they tend to overshoot the value of ρ at which this happens, as was hypothesized in [17]. Our method does not rely on any previously obtained spectrum at ρ to determine the spectrum at $\rho+\Delta\rho$. Instead, at any ρ value, the spectra of an entirely new set of matrices is computed. To the best of our knowledge, finite-difference methods have not been used on this problem. Indeed, using finite-difference methods on this problem does not appear to be a good idea: the number of grid points required for a decent accuracy in this problem seems prohibitive. A comparison of matrix sizes required for equal accuracy using either Hill's method or a finite-difference method is given in [7].

Acknowledgements

The work presented here was sponsored by NSF-DMS-FRG-0351466 (BD), NSERC and PREA grants (DEP), and NSF-DMS-FRG-0139771 (JC). Further, We are grateful to Arnd Scheel for useful discussions regarding Section 5.

References

[1] M. J. Ablowitz and H. Segur. On the evolution of packets of water waves. *J. Fluid Mech.*, 92(4):691–715, 1979.

[2] M. J. Ablowitz and H. Segur. *Solitons and the inverse scattering transform.* Society for Industrial and Applied Mathematics (SIAM), Philadelphia, PA, 1981.

[3] D. Anderson, A. Bondeson, and M. Lisak. Stability analysis of lower-hybrid cones. *Phys. Scripta*, 20(3-4):343–345, 1979.

[4] S. N. Chow and J. K. Hale. *Methods of bifurcation theory.* Springer-Verlag, NY, 1982.

[5] E. A. Coddington and N. Levinson. *Theory of ordinary differential equations.* McGraw-Hill Book Company, Inc., New York-Toronto-London, 1955.

[6] B. I. Cohen, K. M. Watson, and B. J. West. Some properties of deep-water solitons. *Physics of Fluids*, 19(3):345–354, 1976.

[7] B. Deconinck and J. N. Kutz. Computing spectra of linear operators using Hill's method. *Submitted for publication*, 2005.

[8] R. A. Gardner and K. Zumbrun. The gap lemma and geometric criteria for instability of viscous shock profiles. *Comm. Pure Appl. Math.*, 51:797–855, 1998.

[9] J. Hammack. The observation of one-dimensional NLS solitons in deep water. Unpublished results on experiments performed at the University of Florida, 1979.

[10] P. A. E. M. Janssen and J. J. Rasmussen. Nonlinear evolution of the transverse instability of plane-envelope solitons. *Physics of Fluids*, 26:1279–1287, 1983.

[11] T. Kapitula, P. G. Kevrekidis, and B. Sandstede. Counting eigenvalues via the Krein signature in infinite-dimensional Hamiltonian systems. *Phys. D*, 195(3-4):263–282, 2004.

[12] T. Kapitula and B. Sandstede. Stability of bright solitary-wave solutions to perturbed nonlinear Schrödinger equations. *Phys. D*, 124(1-3):58–103, 1998.

[13] T. Kapitula and B. Sandstede. Edge bifurcations for near integrable systems via Evans function techniques. *SIAM J. Math. Anal.*, 33(5):1117–1143, 2002.

[14] Y. S. Kivshar and D. E. Pelinovsky. Self-focusing and transverse instabilities of solitary waves. *Phys. Rep.*, 331(4):117–195, 2000.

[15] E. A. Kuznetsov, A. M. Rubenchik, and V. E. Zakharov. Soliton stability in plasmas and hydrodynamics. *Phys. Rep.*, 142(3):103–165, 1986.

[16] D. U. Martin, H. C. Yuen, and P. G. Saffman. Stability of plane wave solutions of the two-space dimensional nonlinear Schrödinger equation. *Wave Motion*, 2:215–229, 1980.

[17] D. E. Pelinovsky. A mysterious threshold for transverse instability of deep-water solitons. *Math. Comput. Simulation*, 55(4-6):585–594, 2001.

[18] D. E. Pelinovsky. Inertia law for spectral stability of solitary waves in coupled nonlinear Schrödinger equations. *Proc. R. Soc. Lond. Ser. A*, 461(2055):783–812, 2005.

[19] D. E. Pelinovsky, Y. S. Kivshar, and V. V. Afanasjev. Internal modes of envelope solitons. *Phys. D*, 116(1-2):121–142, 1998.

[20] N. R. Pereira, A. Sen, and A. Bers. Non-linear development of lower hybrid cones. *Physics of Fluids*, 21(1):117–120, 1978.

[21] P. G. Saffman and H. C. Yuen. Stability of a plane soliton to infinitesimal two-dimensional perturbations. *Physics of Fluids*, 21:1450–1451, 1978.

[22] D. V. Skryabin. Role of internal and continuum modes in modulational instability of quadratic solitons. *Phys. Rev. E*, 60(6):7511–7517, 1999.

[23] C. Sulem and P.-L. Sulem. *The nonlinear Schrödinger equation.* Springer-Verlag, NY, 1999.

[24] N. Yajima. Stability of envelope soliton. *Prog. Theor. Phys.*, 52:1066–1067, 1974.

[25] H. C. Yuen and B. M. Lake. Nonlinear dynamics of deep-water gravity waves. *Adv. Appl. Mech.*, 22:67–229, 1982.

[26] V. E. Zakharov and A. M. Rubenchik. Instability of waveguides and solitons in nonlinear media. *Sov. Phys. JETP.*, 38(3):494–500, 1974.